

# Observation of Temperature-Independent Anomalous Hall Effect in Thin Bismuth from Near Absolute Zero to 300 K Temperature

Oulin Yu<sup>1</sup>, F. Boivin, A. Silberztein<sup>1</sup>, and G. Gervais<sup>1\*</sup>  
*Department of Physics, McGill University, Montréal, Québec, H3A 2T8, Canada*

 (Received 17 June 2024; revised 24 July 2024; accepted 8 January 2025; published 10 February 2025)

We report our discovery of a temperature-independent anomalous Hall effect (AHE) from 15 mK to 300 K temperature occurring in a pure bismuth transport device whose average thickness is 68 nm. This surprising behavior is accompanied with an expected temperature-dependent longitudinal resistance consistent with semimetallic bismuth. However, it surprisingly showed no hint of a magnetoresistance for magnetic fields between  $\pm 30$  T. Even though bismuth is a diamagnetic material that *a priori* does not break time-reversal symmetry, our analysis of the reconstructed conductivities points toward the AHE to be of the intrinsic type that does not emanate from magnetic impurities. Finally, as pure bismuth has been shown numerically to host a Berry curvature at its surface that breaks inversion symmetry, we propose it as a possible explanation for the temperature-independent AHE observed here.

DOI: [10.1103/PhysRevLett.134.066603](https://doi.org/10.1103/PhysRevLett.134.066603)

*Introduction*—Ever since Faraday’s discovery of its diamagnetism in the mid-nineteenth century, elemental bulk bismuth has been extensively studied and has been a wonder material for exploring new physical properties and phenomena such as the Shubnikov–de Haas (SdH), de Haas–Van Alphen, and Nernst–Etingshausen effects. More recently, there has been a revival of experimental and theoretical work on single crystalline bismuth as it has demonstrated evidence for superconductivity at temperatures below  $T_c \approx 0.5$  mK [1], as well as edge and hinge states that are consistent with models of higher-order topology [2,3]. These discoveries make elemental bismuth an interesting platform for exploring exotic physical properties. For instance, a nonlinear Hall effect was recently discovered in bismuth that showed tunability even at room temperature [4]. Additionally, being a material with high spin-orbit coupling, bismuth is known to host a buckled honeycomb lattice, making it a suitable candidate to study the parity anomaly predicted by Haldane [5].

While bismuth has been extensively studied in its bulk form, the exploration of its two-dimensional form has been limited due to fabrication challenges. Unlike graphite or other group V elements such as black phosphorus, the strong interlayer bonds make it difficult to mechanically exfoliate thin bismuth. Recent works on thin bismuth largely rely on molecular beam epitaxy [6–8] or more creative methods such as the use of nanomolds [9] to press bulk bismuth down to 10 nm. These methods are not widely accessible compared to the simpler mechanical exfoliation, leaving the electronic transport properties of single crystal bismuth below 100 nm largely unexplored. In this Letter,

by making use of a newly developed mechanical exfoliation technique based on microtrenches [10], we successfully fabricated thin bismuth devices and carried out transport measurements in magnetic fields ranging from  $-30$  to  $30$  T, and from near absolute zero to  $300$  K. Strikingly, the anomalous Hall effect (AHE) discovered in our Van der Pauw (VdP) device with an average thickness of  $68$  nm [11] is found to be temperature-independent, while the magnetoresistance is found to be entirely featureless. Both are remarkably surprising given the wide temperature range of investigation and the large applied magnetic fields.

*Anomalous Hall effect*—It is widely accepted in the literature that the total anomalous Hall conductivity (AHC) can be expressed as [12]

$$\sigma_{\text{AHE}} = \sigma_{\text{sk}} + \sigma_{\text{sj}} + \sigma_{\text{int}}, \quad (1)$$

where  $\sigma_{\text{AHE}}$  is the total AHC and  $\sigma_{\text{sk}}$ ,  $\sigma_{\text{sj}}$ ,  $\sigma_{\text{int}}$  are the skew-scattering, side-jump, and intrinsic contributions, respectively. One way to parse the mechanisms responsible for the AHE is to study how the AHC scales with the longitudinal conductivity  $\sigma_{xx}(T)$  [12–15]. Since the skew-scattering and side-jump mechanisms both depend on impurities, the intrinsic contribution is, in principle, the only term that is temperature-independent [16]. A hallmark of the intrinsic contribution  $\sigma_{\text{int}}$  is that it does not scale with the longitudinal conductivity  $\sigma_{xx}(T)$  as described by the semi-empirical relation [12,14]

$$-\sigma_{\text{AHE}}(T) = (\alpha\sigma_{xx0}^{-1} + \beta\sigma_{xx0}^{-2})\sigma_{xx}^2(T) + \sigma_{\text{int}}, \quad (2)$$

where  $\alpha$  and  $\beta$  are coefficients for the skew-scattering and side-jump mechanisms, respectively,  $\sigma_{xx0}$  is the zero-field

\*Contact author: [gervais@physics.mcgill.ca](mailto:gervais@physics.mcgill.ca)

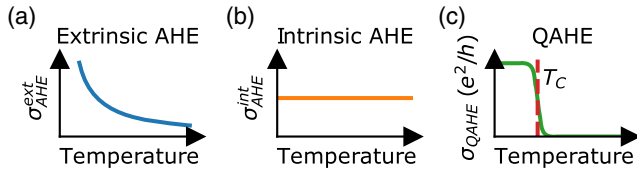


FIG. 1. (a) Example of Hall conductivity due to the extrinsic contributions. Note that the  $\sigma_{\text{AHE}}^{\text{ext}}$  could be increasing or decreasing with temperature depending upon the material [17]. (b) Hall conductivity due to the intrinsic contribution. (c) Below the critical temperature  $T_C$ , the QAHE yields exactly one conductance quantum  $e^2/h$  per edge or surface state.

residual conductivity as  $T \rightarrow 0$ , and  $\sigma_{\text{int}}$  is the intrinsic AHC that remains constant. The expected temperature dependences for the extrinsic and intrinsic dominated AHE are shown in Figs. 1(a) and 1(b), respectively. Depending on the material studied and the temperature range of investigation [17], the extrinsic AHE  $\sigma_{\text{AHE}}^{\text{ext}}$  can increase or decrease with temperature. For comparison, the expected temperature dependence for the quantum anomalous Hall effect (QAHE) is also shown in Fig. 1(c). It is known that the intrinsic AHE is a precursor of the QAHE [14,18,19] that yields an anomalous conductance of exactly  $e^2/h$  per edge or surface state and is temperature-independent below a critical temperature  $T_C$  [20].

*Methods*—Details of the fabrication process and characterizations can be found in the Supplemental Material (SM) [21] and in Yu *et al.* [10], which also includes the AHE observations in two other bismuth devices in a comb geometry with average thicknesses of 29 and 69 nm. The exfoliated bismuth flakes are produced in such way to favor its orientation in the (111) plane, as discussed in the SM. The illustration and the optical image of the VdP device with an average thickness of 68 nm are shown in Figs. 2(a) and 2(b), respectively (see SM for more details). Transport measurements (details found in the SM) are performed in a perpendicular magnetic field with field strengths up to  $\pm 30$  T and temperatures ranging from 1.4 to 300 K in a resistive magnet. The lowest temperature data at  $T = 15$  mK was measured between  $\pm 9$  T in a dilution refrigerator [11], and it showed identical behaviors, although for the remainder of this Letter, we will focus only on the 1.4 to 300 K data as they were taken during a single cooldown.

*Onsager symmetrization*—As shown in Fig. 2(b), the Ohmic contacts deposited on the bismuth flake are located close to one another due to the small size of the flake. An ideal VdP geometry would have the contact electrodes located at each corner of a square sample, as depicted in the insets of Fig. 3, and this is not the case here. Consequently, in our measurements, the Hall ( $R_{xy}$ ) and longitudinal ( $R_{xx}$ ) resistances are inevitably mixed and are measured simultaneously regardless of the probe configuration. To remedy this, we made use of Onsager’s reciprocity theorem [26] to reconstruct the Hall and longitudinal resistances, as discussed in detail in the SM [21].

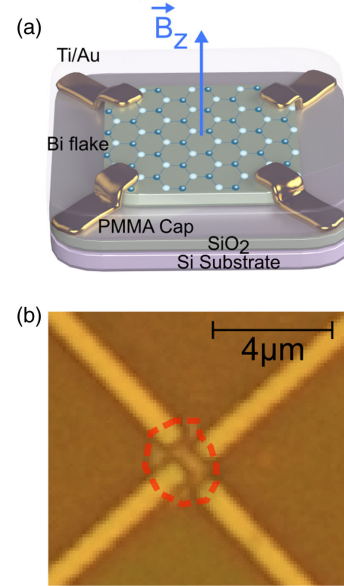


FIG. 2. (a) Schematic of the device with an arrow showing the direction of the applied magnetic field  $\vec{B}_z$ . (b) Optical microscope image of the fabricated device where the flake is circled by the red dashed line.

The resistances as a function of the magnetic field were measured in two different Onsager pairs: one that maximizes the Hall signal ( $XY$  configurations 1 and 2) as shown in Figs. 3(a) and 3(b), and one that maximizes the longitudinal signal ( $XX$  configurations 1 and 2) as shown in Figs. 3(d) and 3(e). The  $XY$  Onsager pair’s data were then antisymmetrized to obtain the Hall resistance, shown in Fig. 3(c). Similarly, the  $XX$  Onsager pair’s data were symmetrized to extract the longitudinal resistance, as shown in Fig. 3(f).

*Hall and longitudinal resistances*—As previously reported [11] and as shown in Fig. 3(c), the AHE is unambiguously observed in our elemental bismuth device. Hints of the AHE occurring in bismuth were reported before in the 1990s by Conn and Donovan [27,28], as well as recently in its bulk form by Camargo *et al.* [29], who eliminated the possibility of magnetic contaminants and speculated that the AHE arises from the surface. In bismuth thin films, the AHE has been demonstrated by Hirai *et al.* in a 30 nm bismuth film where the time-reversal symmetry (TRS) was broken by opening a gap in bismuth’s band structure with intense circularly polarized light [30]. Another more recent instance of this AHE feature was observed by Abdelbarey *et al.* [7] where the authors were unable to explain the nonlinearity near zero field and called it “unusual”.

Interestingly, in Partin *et al.*’s work on molecular beam epitaxy-grown bismuth films [31], although it was overlooked by the authors, their 100 nm film displayed a Hall response and a completely featureless longitudinal response up to 17 T that agree with what we have found

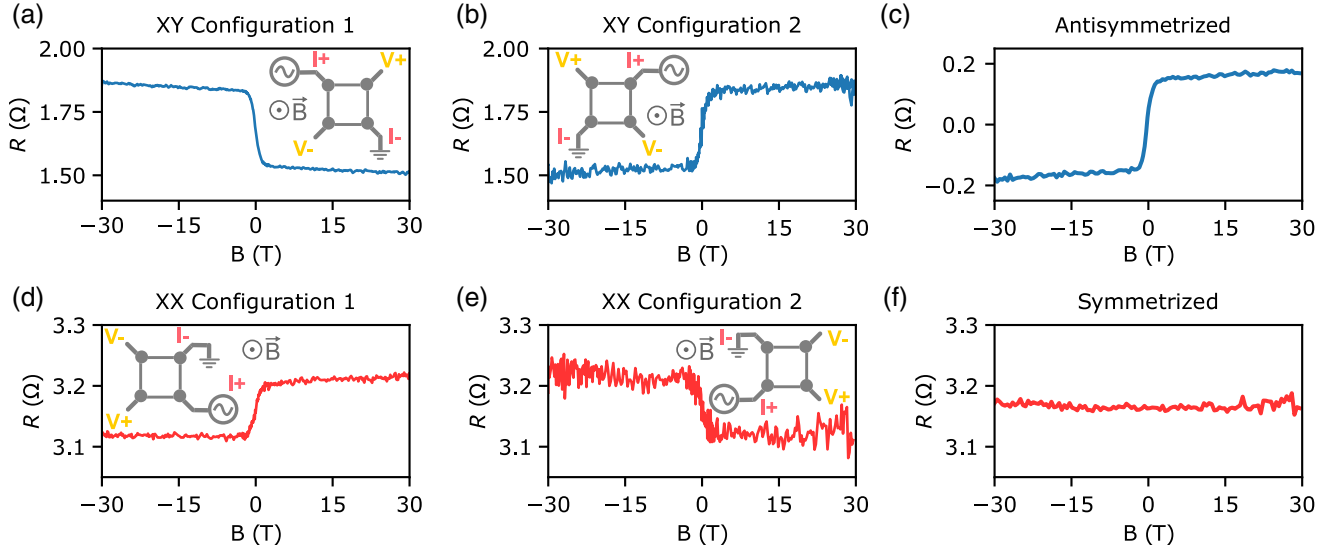


FIG. 3. Resistances as a function of the magnetic field at  $T = 1.4$  K. (a),(b) Onsager configurations optimizing the  $XY$  or Hall measurements. (d),(e) Onsager configurations optimizing the  $XX$  or the longitudinal measurements. (c) Antisymmetrized data that show the extracted Hall resistance from the  $XY$  configurations shown in (a), (b). (f) Symmetrized data that show the extracted longitudinal resistance from the  $XX$  configurations shown in (d),(e). Note that the noise in (c) and (f) is different due to the averaging process required for the antisymmetrization and symmetrization.

in our 68 nm device up to a field of  $\pm 30$  T [see Fig. 3(f)]. While their film is unlikely to be protected by an encapsulating layer, all of our devices are capped by a polymethyl methacrylate layer in order to avoid oxidization and aging. These converging observations indicate that the AHE in elemental bismuth is genuine, yet as of today its exact mechanism remains unclear. Furthermore, it is not yet clear at what critical thickness bismuth thin films would exhibit a predominant AHE, but previous and current data would locate it in the vicinity of 100 nm.

The complete absence of magnetoresistance and SdH oscillations is particularly puzzling since diamagnetic and semimetallic materials typically have a magnetoresistance that scales with  $B^2$  [32–39]. Meanwhile, SdH oscillations were observed in bulk bismuth for magnetic fields as low as 1 T [40], and in a more recent work on growing 10 to 20 nm thin bismuth in nanomolds, at fields as low as 5 T [9]. As pointed out in the SM [21] and in our previous report [11], such observation cannot be explained by a multicarrier model normally applied to bismuth systems. A single-carrier model could yield a constant magnetoresistance, but from the slight slope at high fields seen in Fig. 3(c), the extracted hole density ( $4\text{--}9 \times 10^{22} \text{ cm}^{-3}$  for a 3D model or  $4\text{--}7 \times 10^{17} \text{ cm}^{-2}$  for a 2D model) and hole mobility ( $5\text{--}17 \text{ cm}^2 \text{ V}^{-1} \text{ s}^{-1}$ ) are far from the reported values in the literature [41–47].

*Temperature independence of the AHE in thin bismuth*—The main result of this Letter is shown in Fig. 4. The resistances versus magnetic field for all VdP configurations shown in Fig. 3 were measured at temperatures of 1.4, 40, 80, 160, 240, and 300 K during a single cooldown. The Hall resistances  $R_{xy}$  extracted via antisymmetrization are

shown in the main panel of Fig. 4(a), where the inset shows an enlargement near zero field between  $\pm 2$  T. The same  $R_{xy}$  data is shown in three dimensions in Fig. 4(c). Similarly, the longitudinal resistance extracted from the  $XX$  Onsager pair is plotted in Figs. 4(b) and 4(d). In Fig. 4(d), the zero field ( $B = 0$  T) temperature dependence of  $R_{xx}(T)$  for the  $XX$  configuration 1 between 3 and 260 K is shown in gray in the background. This increasing resistance with increasing temperature is consistent with the semimetallic nature of bulk and thin bismuth [31,46,47].

Most strikingly, our data shown in Figs. 4(a) and 4(c) demonstrates the observed AHE to be, within noise, entirely independent of temperature. The negligible temperature dependence is particularly notable in the low field region of  $|B| < 2$  T, where the  $R_{xy}(B)$  data completely overlap for all temperatures investigated. This was further verified down to 15 mK in a dilution refrigerator during a separate cooldown. In the high field regions where the AHE is saturated, the anomalous Hall resistance  $R_{\text{AHE}}$  can be extracted via the zero-field intercept of a linear fit (see SM [21]). At first sight, this lack of temperature dependence may seem surprising. However, an important feature of the intrinsic AHE is that it is temperature-independent [12,14], as illustrated in Fig. 1(b). This is further expected in our case since the estimated longitudinal conductivity of our device is in the good-metal regime  $\sigma_{xx} \sim 10^4\text{--}10^6 \text{ } \Omega^{-1} \text{ cm}^{-1}$  which is typical for materials exhibiting an AHE that is intrinsic in nature [14]. Furthermore, our analysis on the relation found in Eq. (2) (see SM) shows the proper linear scaling between  $-\sigma_{\text{AHE}}$  and  $\sigma_{xx}^2$ , further pointing the observed AHE toward the intrinsic type.

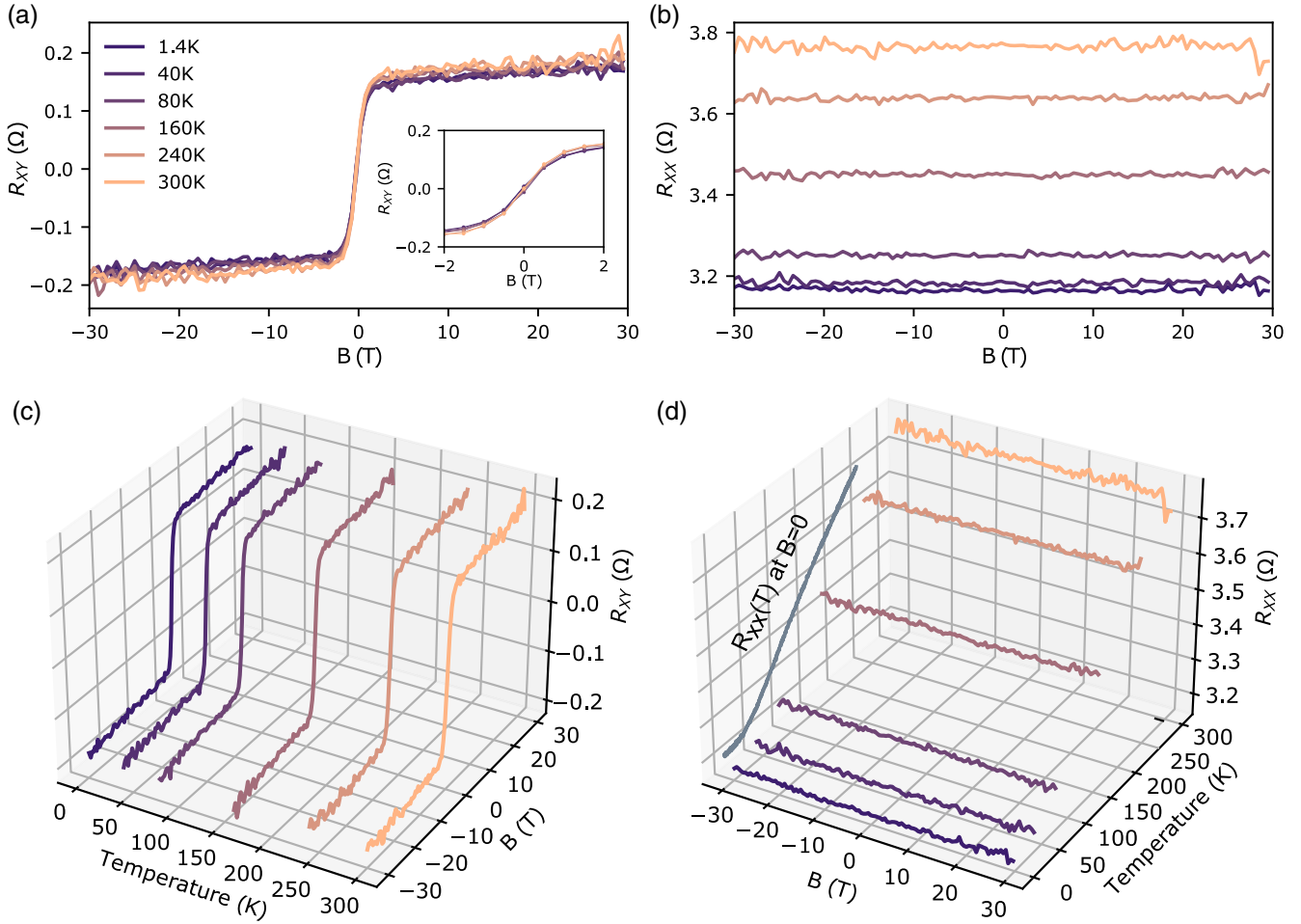


FIG. 4. (a) Hall and (b) longitudinal resistances as a function of the magnetic field at various temperatures ranging from 1.4 to 300 K. The inset in (a) is an enlargement for the data between  $\pm 2$  T. (c),(d) 3D plots of the same curves in (a) and (b), respectively. The longitudinal resistance  $R_{xx}(T)$  for the XX configuration 1 is shown in the background of (d) for comparison.

The underlying mechanism of the AHE in bismuth is in our view unlikely due to magnetism of any kind given the lack of temperature dependence. Furthermore, and as discussed in the SM [21], elemental bismuth is known to be a diamagnetic material that *a priori* does not break TRS, and has a relatively weak temperature-dependent susceptibility that varies by a factor of 2 from 540 K to low temperatures [48]. In contrast, an intrinsic AHE can originate from a nonzero Berry curvature [13,14] with the necessary condition of breaking either TRS or inversion symmetry [49]. In bismuth, inversion symmetry is preserved in the bulk but broken at the surface [50], a nonzero Berry curvature could thus be present at the surface without breaking TRS. Recent first principle calculations by Wawrzik *et al.* [51] confirmed this by showing that while bismuth has a zero Berry curvature in the bulk, its surface nevertheless hosts a nonzero Berry curvature. This serves as the basis for understanding the room temperature nonlinear Hall effect observed very recently by Makushko *et al.* [4]. We propose that bismuth's nonzero Berry curvature at its

surface could explain the temperature-independent AHE observed in our Letter. Future theoretical and experimental work is therefore required to further understand and unravel the exact mechanism at play.

*Conclusion*—In this Letter, we measured the resistances of a bismuth transport device with an average thickness of 68 nm in different VdP configurations up to  $\pm 30$  T and between 15 mK to 300 K. The extracted longitudinal resistance was observed to be completely featureless for all investigated temperatures. The extracted Hall resistance clearly demonstrates an anomaly consistent with the anomalous Hall effect, and was observed to be entirely independent of temperature. Most, if not all mechanisms, except for the Berry curvature responsible for the intrinsic AHE, are temperature-dependent in the range of investigation. We are unaware of any model that could explain simultaneously the observed Hall and longitudinal signals, nor any other material that exhibits an electronic Hall transport that is so insensitive to temperature for such a wide range. This makes bismuth an intriguing material that

is still not well understood. Looking forward, given the intrinsic AHE is the precursor of QAHE, we speculate whether bismuth could be a suitable platform to explore the QAHE given its buckled honeycomb crystal structure and high spin-orbit coupling, both being important ingredients for the parity anomaly predicted by Haldane [5]. If this is the case in bismuth, then this also raises the fascinating question of whether the QAHE could be observable at much higher temperatures than it currently is.

*Acknowledgments*—This work has been supported by the New Frontiers in Research Fund program, the Natural Sciences and Engineering Research Council of Canada, the Canadian Foundation for Innovation, the Fonds de Recherche du Québec Nature et Technologies and Montréal-based CXC. Sample fabrication was carried out at the McGill Nanotools Microfabrication facility and at the Laboratoire de Microfabrication at Polytechnique Montréal. A portion of this work was performed at the National High Magnetic Field Laboratory, which is supported by National Science Foundation Cooperative Agreement No. DMR-2128556\* and the State of Florida. We are grateful to M.-O. Goerbig and T. Szkopek for the extremely helpful discussions and comments, as well as for the reading of the manuscript. Finally, we would like to thank R. Talbot, R. Gagnon, J. Smeros and S. Chikara for technical assistance.

- [1] O. Prakash, A. Kumar, A. Thamizhavel, and S. Ramakrishnan, Evidence for bulk superconductivity in pure bismuth single crystals at ambient pressure, *Science* **355**, 52 (2017).
- [2] L. Aggarwal, P. Zhu, T.L. Hughes, and V. Madhavan, Evidence for higher order topology in Bi and  $\text{Bi}_{0.92}\text{Sb}_{0.08}$ , *Nat. Commun.* **12**, 4420 (2021).
- [3] F. Schindler, Z. Wang, M.G. Vergniory, A.M. Cook, A. Murani, S. Sengupta, A. Y. Kasumov, R. Deblock, S. Jeon, I. Drozdov, H. Bouchiat, S. Guéron, A. Yazdani, B. A. Bernevig, and T. Neupert, Higher-order topology in bismuth, *Nat. Phys.* **14**, 918 (2018).
- [4] P. Makushko, S. Kovalev, Y. Zabala, I. Ilyakov, A. Ponomaryov, A. Arshad, G.L. Prajapati, T.V.A.G. de Oliveira, J.-C. Deinert, P. Chekhonin, I. Veremchuk, T. Kosub, Y. Skourski, F. Ganss, D. Makarov, and C. Ortix, A tunable room-temperature nonlinear Hall effect in elemental bismuth thin films, *National electronics review* **7**, 207 (2024).
- [5] F.D.M. Haldane, Model for a quantum Hall effect without Landau levels: Condensed-matter realization of the “parity anomaly”, *Phys. Rev. Lett.* **61**, 2015 (1988).
- [6] S.-Y. Yang, K. Chang, and S. S. P. Parkin, Large planar Hall effect in bismuth thin films, *Phys. Rev. Res.* **2**, 022029(R) (2020).
- [7] D. Abdelbarey, J. Koch, Z. Mamiyev, C. Tegenkamp, and H. Pfnür, Thickness-dependent electronic transport through epitaxial nontrivial Bi quantum films, *Phys. Rev. B* **102**, 115409 (2020).
- [8] D. Abdelbarey, J. Koch, P. Kröger, P. Yogi, C. Tegenkamp, and H. Pfnür, Magnetoconductance in epitaxial bismuth quantum films: Beyond weak (anti)localization, *Phys. Rev. B* **104**, 075431 (2021).
- [9] L. Chen, A. X. Wu, N. Tulu, J. Wang, A. Juanson, K. Watanabe, T. Taniguchi, M. T. Pettes, M. A. Campbell, M. Xu, C. A. Gadre, Y. Zhou, H. Chen, P. Cao, L. A. Jauregui, R. Wu, X. Pan, and J. D. Sanchez-Yamagishi, Exceptional electronic transport and quantum oscillations in thin bismuth crystals grown inside van der Waals materials, *Nat. Mater.* **23**, 741 (2024).
- [10] O. Yu, R. Allgayer, S. Godin, J. Lalande, P. Fossati, C. Hsu, T. Szkopek, and G. Gervais, Method of mechanical exfoliation of bismuth with micro-trench structures, *J. Appl. Phys.* **134**, 244302 (2023).
- [11] O. Yu, S. Vijaykrishnan, R. Allgayer, T. Szkopek, and G. Gervais, Anomalous Hall effect in thin bismuth, *Phys. Rev. B* **109**, L121406 (2024).
- [12] Y. Tian, L. Ye, and X. Jin, Proper scaling of the anomalous Hall effect, *Phys. Rev. Lett.* **103**, 087206 (2009).
- [13] D. Culcer, in *Encyclopedia of Condensed Matter Physics (Second Edition)*, edited by T. Chakraborty (Academic Press, New York, 2024), Vol. 1, p. 587.
- [14] N. Nagaosa, J. Sinova, S. Onoda, A. H. MacDonald, and N. P. Ong, Anomalous Hall effect, *Rev. Mod. Phys.* **82**, 1539 (2010).
- [15] S. Onoda, N. Sugimoto, and N. Nagaosa, Intrinsic versus extrinsic anomalous Hall effect in ferromagnets, *Phys. Rev. Lett.* **97**, 126602 (2006).
- [16] A. Shitade and N. Nagaosa, Anomalous Hall effect in ferromagnetic metals: Role of phonons at finite temperature, *J. Phys. Soc. Jpn.* **81**, 083704 (2012).
- [17] T. Miyasato, N. Abe, T. Fujii, A. Asamitsu, S. Onoda, Y. Onose, N. Nagaosa, and Y. Tokura, Crossover behavior of the anomalous Hall effect and anomalous Nernst effect in itinerant ferromagnets, *Phys. Rev. Lett.* **99**, 086602 (2007).
- [18] H. Weng, R. Yu, X. Hu, X. Dai, and Z. Fang, Quantum anomalous Hall effect and related topological electronic states, *Adv. Phys.* **64**, 227 (2015).
- [19] C.-X. Liu, S.-C. Zhang, and X.-L. Qi, The quantum anomalous Hall effect: Theory and experiment, *Annu. Rev. Condens. Matter Phys.* **7**, 301 (2016).
- [20] C.-Z. Chang, C.-X. Liu, and A. H. MacDonald, Colloquium: Quantum anomalous Hall effect, *Rev. Mod. Phys.* **95**, 011002 (2023).
- [21] See Supplemental Material at <http://link.aps.org/supplemental/10.1103/PhysRevLett.134.066603>, which includes Refs. [22–25], for additional information about the device fabrication, characterization, experimental methods, extraction of the anomalous Hall resistance, and detailed discussions on its temperature dependence.
- [22] Q. Lu *et al.*, Observation of 2D Weyl fermion states in epitaxial bismuthene, *arXiv:2303.02971*.
- [23] A. A. Burkov, Anomalous Hall effect in Weyl metals, *Phys. Rev. Lett.* **113**, 187202 (2014).
- [24] Y. Messica, D. B. Gutman, and P. M. Ostrovsky, Anomalous Hall effect in disordered Weyl semimetals, *Phys. Rev. B* **108**, 045121 (2023).
- [25] Z. Zhu, B. Fauqué, K. Behnia, and Y. Fuseya, Magneto-resistance and valley degree of freedom in bulk bismuth, *J. Phys. Condens. Matter* **30**, 313001 (2018).

- [26] H. H. Sample, W. J. Bruno, S. B. Sample, and E. K. Sichel, Reverse-field reciprocity for conducting specimens in magnetic fields, *J. Appl. Phys.* **61**, 1079 (1987).
- [27] B. Donovan and G. Conn, LXIX. The electrical conductivity of bismuth fibres: II. Anomalies in the magneto-resistance, *London Edinburgh Dublin Philos. Mag. J. Sci.* **41**, 770 (1950).
- [28] G. K. T. Conn and B. Donovan, Anomalous magneto-resistance effects in bismuth, *Nature (London)* **162**, 336 (1948).
- [29] B. C. Camargo, P. Gierlowski, A. Alaferdov, I. N. Demchenko, M. Sawicki, K. Gas, and Y. Kopelevich, Anomalous Hall effect in bismuth, *J. Magn. Magn. Mater.* **525**, 167581 (2021).
- [30] Y. Hirai, N. Yoshikawa, M. Kawaguchi, M. Hayashi, S. Okumura, T. Oka, and R. Shimano, Anomalous Hall effect of light-driven three-dimensional Dirac electrons in bismuth, [arXiv:2301.06072](https://arxiv.org/abs/2301.06072).
- [31] D. L. Partin, J. Heremans, D. T. Morelli, C. M. Thrush, C. H. Olk, and T. A. Perry, Growth and characterization of epitaxial bismuth films, *Phys. Rev. B* **38**, 3818 (1988).
- [32] M. Cabrera-Baez, K. V. R. A. Silva, P. R. T. Ribeiro, D. R. Ratkovski, E. L. T. França, A. Flessa-Savvidou, B. Casas, T. Siegrist, L. Balicas, S. M. Rezende, and F. L. A. Machado, Giant magnetoresistance in the crystalline YCd<sub>6</sub> intermetallic compound, *Phys. Rev. B* **107**, 144414 (2023).
- [33] J. Juraszek, L. Bochenek, A. Rudenko, M. M. Hosen, M. Daszkiewicz, Z. Wang, J. Wosnitza, Z. Henkie, M. Samsel-Czekala, M. Neupane, and T. Cichorek, Nonsaturating extreme magnetoresistance and large electronic magnetostriction in LuAs, *Phys. Rev. Res.* **1**, 032016(R) (2019).
- [34] I. A. Leahy, Y.-P. Lin, P. E. Siegfried, A. C. Treglia, J. C. W. Song, R. M. Nandkishore, and M. Lee, Nonsaturating large magnetoresistance in semimetals, *Proc. Natl. Acad. Sci. U.S.A.* **115**, 10570 (2018).
- [35] T. Liang, Q. Gibson, M. N. Ali, M. Liu, R. J. Cava, and N. P. Ong, Ultrahigh mobility and giant magnetoresistance in the Dirac semimetal Cd<sub>3</sub>As<sub>2</sub>, *Nat. Mater.* **14**, 280 (2014).
- [36] M. N. Ali, J. Xiong, S. Flynn, J. Tao, Q. D. Gibson, L. M. Schoop, T. Liang, N. Haldolaarachchige, M. Hirschberger, N. P. Ong, and R. J. Cava, Large, non-saturating magnetoresistance in WTe<sub>2</sub>, *Nature (London)* **514**, 205 (2014).
- [37] C. Shekhar, A. K. Nayak, Y. Sun, M. Schmidt, M. Nicklas, I. Leermakers, U. Zeitler, Y. Skourski, J. Wosnitza, Z. Liu, Y. Chen, W. Schnelle, H. Borrmann, Y. Grin, C. Felser, and B. Yan, Extremely large magnetoresistance and ultrahigh mobility in the topological Weyl semimetal candidate NbP, *Nat. Phys.* **11**, 645 (2015).
- [38] N. Kumar, Y. Sun, N. Xu, K. Manna, M. Yao, V. Süß, I. Leermakers, O. Young, T. Förster, M. Schmidt, H. Borrmann, B. Yan, U. Zeitler, M. Shi, C. Felser, and C. Shekhar, Extremely high magnetoresistance and conductivity in the type-II Weyl semimetals WP<sub>2</sub> and MoP<sub>2</sub>, *Nat. Commun.* **8**, 1642 (2017).
- [39] F. F. Tafti, Q. D. Gibson, S. K. Kushwaha, N. Haldolaarachchige, and R. J. Cava, Resistivity plateau and extreme magnetoresistance in LaSb, *Nat. Phys.* **12**, 272 (2015).
- [40] L. S. Lerner, Shubnikov-de Haas effect in bismuth, *Phys. Rev.* **127**, 1480 (1962).
- [41] A. L. Jain, S. Suri, and K. Tanaka, Charge carrier densities and mobilities in bismuth, *Phys. Lett.* **28A**, 435 (1968).
- [42] A. L. Jain and S. H. Koenig, Electrons and holes in bismuth, *Phys. Rev.* **127**, 442 (1962).
- [43] S. Kochowski and A. Opilski, Concentration and mobility of charge carriers in thin polycrystalline films of bismuth, *Thin Solid Films* **48**, 345 (1978).
- [44] F. Gity, L. Ansari, M. Lanius, P. Schüffelgen, G. Mussler, D. Grützmacher, and J. C. Greer, Reinventing solid state electronics: Harnessing quantum confinement in bismuth thin films, *Appl. Phys. Lett.* **110**, 093111 (2017).
- [45] Y. Zabala, M. Marszalek, M. Krupinski, A. Zarzycki, and M. Perzanowski, Magnetotransport properties of semi-metallic bismuth thin films for flexible sensor applications, *Coatings* **11**, 175 (2021).
- [46] R. A. Hoffman and D. R. Frankl, Electrical transport properties of thin bismuth films, *Phys. Rev. B* **3**, 1825 (1971).
- [47] C. A. Kukkonen and K. F. Sohn, The low-temperature electrical resistivity of bismuth, *J. Phys. F* **7**, L193 (1977).
- [48] S. Otake, M. Momiuchi, and N. Matsuno, Temperature dependence of the magnetic susceptibility of bismuth, *J. Phys. Soc. Jpn.* **49**, 1824 (1980).
- [49] D. Xiao, M.-C. Chang, and Q. Niu, Berry phase effects on electronic properties, *Rev. Mod. Phys.* **82**, 1959 (2010).
- [50] P. Hofmann, The surfaces of bismuth: Structural and electronic properties, *Prog. Surf. Sci.* **81**, 191 (2006).
- [51] D. Wawrzika, J. I. Facioa, and J. van den Brink, Surface induced electronic Berry curvature in bulk Berry curvature free materials, *Mater. Today Phys.* **33**, 101027 (2023).